Acta Crystallographica Section B
Structural Science
ISSN 0108-7681

Structure of compounds $E(SnMe_3)_4$ (E = Si, Ge) as seen by high-resolution X-ray powder diffraction and solid-state NMR

Robert E. Dinnebier,[a]*† Piotr Bernatowicz,[b] Xavier Helluy,[c] Angelika Sebald,[c] Markus Wunschel,[a] Andy Fitch[d] and Sander van Smaalen[a]

[a]Lehrstuhl für Kristallographie, Universität Bayreuth, D-95440 Bayreuth, Germany, [b]Institute of Organic Chemistry, Polish Academy of Sciences, PO Box 8, PL-01-224 Warsaw 42, Poland, [c]Bayerisches Geoinstitut, Universität Bayreuth, D-95440 Bayreuth, Germany, and [d]ESRF, BP220, F-38043 Grenoble CEDEX, France

† Present address: Max-Planck Institut für Festkörperforschung, Heisenbergstrasse 1, D-70569 Stuttgart, Germany.

Correspondence e-mail: r.dinnebier@fkf.mpg.de

Received 21 May 2001
Accepted 8 October 2001

The compounds tetrakis(trimethylstannyl)germane, $Ge(SnMe_3)_4$ (1), and tetrakis(trimethylstannyl)silane, $Si(SnMe_3)_4$ (2), have crystal structures with the quasispherical molecules in a closed-packed stacking. At room temperature both structures have the space group $P\bar{1}$ (Z = 2) with a = 9.94457 (5), b = 14.52927 (8), c = 9.16021 (5) Å, α = 90.53390 (30), β = 111.73080 (30), γ = 90.0049 (4)°, and V = 1229.414 (12) Å^3 for (1) and a = 9.92009 (7), b = 14.51029 (11), c = 9.13585 (7) Å, α = 90.4769 (4), β = 111.6724 (4), γ = 89.9877 (6)°, and V = 1222.037 (16) Å^3 for (2). The molecules are found to be ordered as a result of steric interactions between neighboring molecules, as shown by analyzing the distances between the atoms. Upon heating, both compounds undergo a first-order phase transition at temperatures T_c = 348 ± 5 K, as characterized by a relative jump of the lattice parameter of ∼16%. At 353 K, both structures have the space group $P\bar{1}$ (Z = 4), with a = 14.2037 (2) Å, and V = 2865.52 (7) Å^3 for (1) and a = 14.1346 (2) Å, and V = 2823.90 (7) Å^3 for (2). Rietveld refinements were performed for the low-temperature phases measured at T = 295 K [R_{wp} = 0.0844 for (1), R_{wp} = 0.0940 for (2)] and for the high-temperature phases measured at T = 353 K [R_{wp} = 0.0891 for (1), R_{wp} = 0.0542 for (2)]. The combination of high-resolution X-ray powder diffraction measurements and variable-temperature magic-angle-spinning ^{13}C, ^{29}Si and ^{119}Sn NMR experiments demonstrates low crystallographic and molecular (C_1) symmetries for the low-temperature phases of (1) and (2) at temperatures T < 348 ± 5 K and high crystallographic symmetry due to rotational disorder for the high-temperature phases at temperatures T > 348 ± 5 K.

1. Introduction

Molecules $E(XMe_3)_4$ (E = C, Si,...; X = C, Si, Sn,...) are almost spherically shaped and non-polar. Therefore, they are prone to dynamic rotational disorder in the solid state. Crystals of this type of molecule exhibit structural phase transitions from predominantly ordered low-temperature phases to increasingly dynamically disordered high-temperature phases at increasing temperatures (Parsonage & Staveley, 1978). Dynamic features include whole-molecule reorientational jumps in the crystal structure and/or individual $2\pi/3$ reorientation of the XMe_3 groups around the $E-X$ bond directions. High-resolution solid-state NMR and X-ray diffraction measurements form an ideal combination of experimental tools to characterize the structural and dynamical properties of these solid phases. X-ray diffraction provides unambiguous information about the lattice, the symmetry and the packing of the quasi-spherical molecules, while NMR can provide infor-

Table 1
Crystallographic data for the low- (LT) and high-temperature (HT) phases of $Ge(SnMe_3)_4$ (1) and $Si(SnMe_3)_4$ (2).

R_p and R_{wp} refer to the Rietveld criteria (Rietveld, 1969) of fit for profile and weighted profile, respectively, defined by Langford & Louër (1996)

	$Ge(SnMe_3)_4$ (1)		$Si(SnMe_3)_4$ (2)	
	LT phase	HT phase	LT phase	HT phase
Formula	$Ge(Sn(CH_3)_3)_4$	$Ge(Sn(CH_3)_3)_4$	$Si(Sn(CH_3)_3)_4$	$Si(Sn(CH_3)_3)_4$
Temperature (K)	295	353	295	353
Formula weight (g mol^{-1})	727.93	727.93	683.41	683.41
Space group	$P\bar{1}$	$Fm\bar{3}m$	$P\bar{1}$	$Fm\bar{3}m$
Z	2	4	2	4
a (Å)	9.94457 (5)	14.2037 (2)	9.92009 (7)	14.1346 (2)
b (Å)	14.52927 (8)	14.2037 (2)	14.51029 (11)	14.1346 (2)
c (Å)	9.16021 (5)	14.2037 (2)	9.13585 (7)	14.1346 (2)
α (°)	90.53390 (30)	90	90.4769 (4)	90
β (°)	111.73080 (30)	90	111.6724 (4)	90
γ (°)	90.0049 (4)	90	89.9877 (6)	90
V (Å^3)	1229.414 (12)	2865.52 (7)	1222.037 (16)	2823.90 (7)
Wavelength (Å)	0.491213 (2)	0.14665	0.491213 (2)	0.14665
R_p (R_p LeBail)	6.65 (5.55)	12.90	6.51 (4.43)	10.7
R_{wp} (R_{wp} LeBail)	8.44 (7.19)	8.91	9.40 (8.47)	5.42
R_F	10.3	6.33	10.6	4.3
χ^2	0.76	1.76	2.43	0.46
No of refined parameters	55	5	55	7
No. of reflections	3021	127	3608	127
μ (cm^{-1})	17.51	2.69	13.49	2.62
ρ_{calc} (g cm^{-3})	1.966	1.687	1.857	1.607
2θ range (°)	−7.878 – 53.016	0.600–8.987	−7.878 – 53.016	0.600–8.987
Step size (°2θ)	0.003 after rebinning	0.0113	0.003 after rebinning	0.0113

mation on the molecular geometries and is very sensitive to variations in both molecular symmetry and dynamics.

The crystal structures, structural phase transitions and molecular dynamics properties of $C(SiMe_3)_4$ and $Si(SiMe_3)_4$ have recently been investigated (Helluy *et al.*, 1998; Dinnebier *et al.*, 1999; Dinnebier, Carlson & van Smaalen, 2000). At room temperature $C(SiMe_3)_4$ and $Si(SiMe_3)_4$ crystallize in space group $Fm\bar{3}m$ (high-temperature phases). At $T < 225$ K both compounds exist in their respective, orientationally ordered low-temperature phases (isostructural, space group $P2_13$, molecular point-group symmetry C_3). While $Si(SiMe_3)_4$ undergoes a direct transition from its high-temperature to its low-temperature phase, an intermediate phase in the temperature range $T = 225$–268 K (space group $Pa\bar{3}$) is found for $C(SiMe_3)_4$ (Dinnebier *et al.*, 1999). The molecular dynamic properties of $C(SiMe_3)_4$ and $Si(SiMe_3)_4$ in their low-temperature phases have been quantitatively characterized by one- and two-dimensional ^{13}C and ^{29}Si magic-angle spinning (MAS) NMR recently (Helluy *et al.*, 1998). In their low-temperature phases both compounds undergo whole-molecule reorientational jumps around the preferred molecular $E-X$ axes, but additional internal $2\pi/3$ reorientations of the $SiMe_3$ groups occur in $Si(SiMe_3)_4$. A different set of structural and dynamic properties is found for $C(SnMe_3)_4$, which, at $T = 173$ K, is known to crystallize in space group $Pa\bar{3}$ and to display a pseudo-fivefold orientational disorder, with the Sn atoms occupying the 20 corners of a nearly regular pentagonal dodecahedron centered on the central C atom in the $C(SnMe_3)_4$ molecule (Klinkhammer *et al.*, 1995). This phase of $C(SnMe_3)_4$ persists up to at least $T = 300$ K, and one- and two-dimensional ^{119}Sn and ^{13}C NMR experiments identify and further characterize the dynamic origin of disorder in this phase of $C(SnMe_3)_4$, where large- and small-angle reorientational jumps of $C(SnMe_3)_4$ molecules in the crystal structure occur with similar exchange rate constants (Bernatowicz *et al.*, 1999).

Although compounds of the type $E(XMe_3)_4$ have similar molecular shapes, their structural and dynamic solid-state properties can differ widely. However, some common trends do exist. One of these trends is that the high molecular symmetry adopted by compounds $E(XMe_3)_4$ in the gas phase (point group T_d: Beagley *et al.*, 1988, 1989) is not preserved in the crystalline low-temperature phases. The low-temperature phases of solid $Ge(SnMe_3)_4$ and $Si(SnMe_3)_4$ have recently been investigated by IR, UV and Raman spectroscopy, where order–disorder phase transitions were observed at $T = 337 \pm 1$ K for $Ge(SnMe_3)_4$, and at $T = 339 \pm 2$ K for $Si(SnMe_3)_4$ (Leites *et al.*, 1999). Except for $C(SnMe_3)_4$ (Klinkhammer *et al.*, 1995), no single crystals of the solvent-free compounds $E(XMe_3)_4$ suitable for single-crystal diffraction experiments could be synthesized so far, leaving

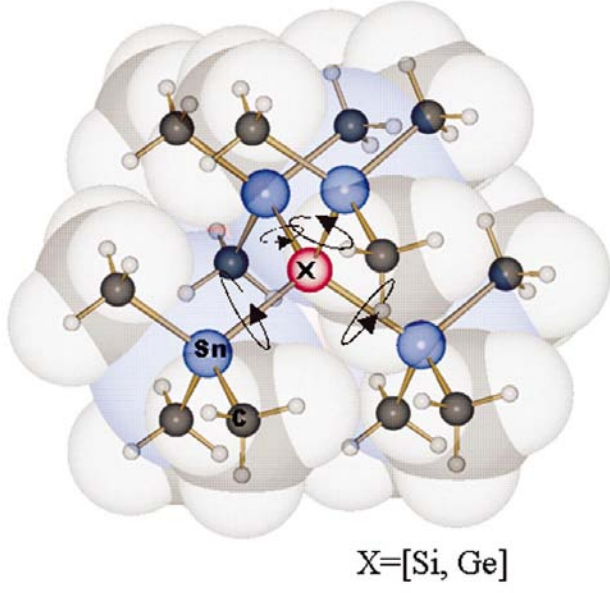

Figure 1
Cup model with ball-and-stick representation inside $E(SnMe_3)_4$, E = Ge (1), Si (2). The four torsion angles of the trimethylstannyl, $SnMe_3$ groups are indicated by arrows.

powder diffraction as the only source of information about the crystal structure.

Here we consider the structural properties of the low- and high-temperature phases of $Ge(SnMe_3)_4$ (1) and $Si(SnMe_3)_4$ (2) (Fig. 1) by means of high-resolution X-ray powder diffraction and solid-state ^{13}C, ^{29}Si and ^{119}Sn NMR experiments. We demonstrate that both solid-state NMR and X-ray diffraction results are incompatible with molecular point-group symmetry T_d for the low-temperature phases of (1) and (2). Our results contradict the earlier interpretation of Raman spectra of solid (1) and (2), as indicative of molecular point-group symmetry T_d (Leites *et al.*, 1999).

2. Experimental

2.1. Materials and methods

2.1.1. Samples. $Ge(SnMe_3)_4$ (1) was synthesized in analogy to the procedure for $C(SnMe_3)_4$ published by Klinkhammer *et al.* (1995) by the reaction of $GeCl_4$ with 4 equiv. of Me_3SnLi in tetrahydrofurane at T = 248 K. After recrystallization from pentane, chemically pure (1) was obtained according to solution-state ^1H, ^{13}C and ^{119}Sn NMR. To obtain a good quality micro-crystalline sample (1) was subsequently sublimed at T = 408 K *in vacuo* (overall yield 16%, m.p. 559–563 K). Our sample of $Si(SnMe_3)_4$ (2) was provided by L. A. Leites and V. Ya. Lee, Moscow.

2.1.2. X-ray powder diffraction. X-ray powder diffraction data were collected at the high-resolution X-ray powder diffractometer at BM16 at the European Synchrotron Radiation Facility (ESRF; Fig. 2). The X-rays from the bending magnet source were collimated vertically by a rhodium-coated silicon mirror before they are incident on the double crystal monochromator. A Si (111) reflection was used to select an X-ray energy of 24 keV. The size of the beam was adjusted to 2 × 0.6 mm^2 using slits. The wavelength was determined to 0.491213 (2) Å from a silicon standard. The samples were contained in 0.7 mm lithium borate glass (glass No. 50) capillaries. The samples were spun during measurements in order to improve randomization of the crystallites. The diffracted beam was analyzed with a nine crystal analyzer stage [nine Ge(111) crystals separated by 2° intervals] and detected with nine Na(Tl)I scintillation counters simultaneously. The incoming beam was monitored by an ion-chamber for normalization of the decay of the primary beam. In this parallel beam configuration, the resolution is determined by the analyzer crystal rather than by the slits (Cox, 1991). Details of the experimental setup are described in the beamline handbook. Data were taken at room temperature in a continuous scanning mode for several hours and they were normalized against monitor counts and detector efficiency and converted to step scan data in steps of 0.003° 2θ. Experimental details for the different samples are given in Table 1. Low-angle diffraction peaks showed a FWHM of 0.007° 2θ for (2) and 0.008° 2θ for (1), still significantly broader than the resolution of the spectrometer which is estimated to be as low as 0.002° 2θ for the selected wavelength. A very small amount of an unidentified additional phase (< 0.5%) with slightly broader peak shapes was observed in several peaks in both powder patterns. Data reduction was performed using the program *GUFI* (Dinnebier & Finger, 1998).

X-ray powder diffraction data of (1) and (2) at high temperature were collected in transmission geometry with a hot air blower mounted on a motorized goniometer head at the insertion device high-energy beamline ID15B at the European Synchrotron Radiation Facility (ESRF; Fig. 3). X-rays of energy 90 keV were selected by a bent Si (511) monochromator which focuses the beam in the horizontal plane (Suortti *et al.*, 2001). The size of the beam was adjusted to several mm height and a width of 0.5 mm. Details of the experimental setup are described in the beamline handbook. A MAR 345 image plate reader was used as the detector at a distance of ∼730 mm from the sample. The wavelength was determined to be 0.14668 (2) Å from an NBS-676 LaB_6 stan-

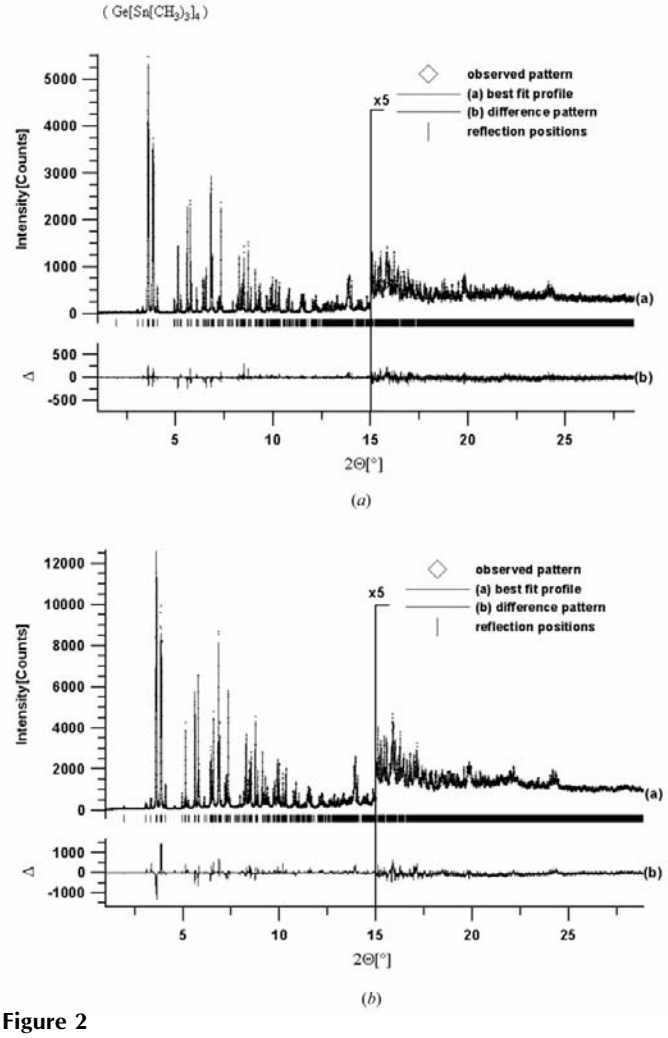

Figure 2
Scattered X-ray intensity for (*a*) $Ge(SnMe_3)_4$ (1) and (*b*) $Si(SnMe_3)_4$ (2) at ambient conditions as a function of diffraction angle 2θ. Shown are the observed patterns (diamonds), the best Rietveld-fit profiles (line) and the enlarged difference curves between observed and calculated profiles in an additional window below. The high-angle parts are enlarged by a factor of 5, starting at 15° 2θ. The wavelength was λ = 0.491213 (2) Å.

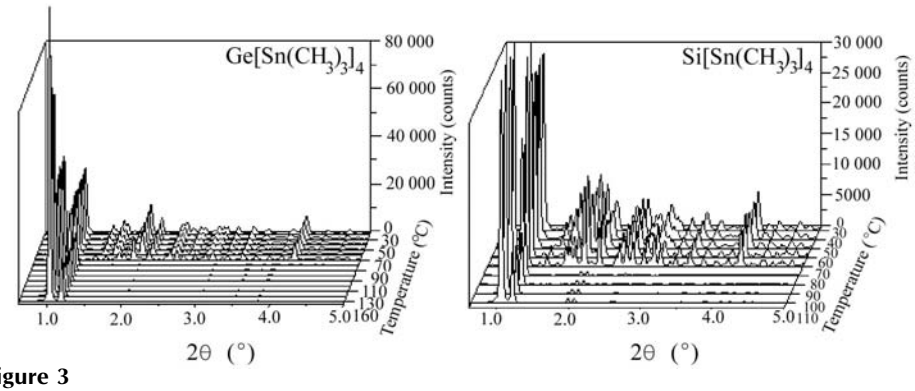

Figure 3
Powder patterns of (1) (right) and (2) (left) in dependence of the temperature in a three-dimensional representation. The first-order phase transition around 343 K (70°C) is clearly visible. Different scales are used for the phases.

dard. The samples were contained in 0.7 mm lithium borate glass (glass No. 50) capillaries and were rocked for several degrees during measurements in order to improve randomization of the crystallites. Data were taken at various temperatures between 298 and 523 K for (2) and between 298 and 403 K for (1). Exposure times between 30 s and 1 min were chosen. Data reduction was performed using the program *FIT2D* (Hammersley, 1997, 1998), resulting in diagrams of corrected intensities *versus* the scattering angle 2θ. The diffracted intensity was observed to be quite uniformly distributed over the Debye–Scherrer rings, ruling out severe grain size effects and preferred orientation. Low-angle diffraction peaks had a FWHM of 0.04° 2θ for (1) and (2), which can be considered as the highest resolution for this particular setup.

2.1.3. Solid-state NMR experiments. One- and two-dimensional ^{13}C, ^{29}Si and ^{119}Sn cross-polarization (CP) MAS and static NMR experiments were recorded on a Bruker MSL 300 NMR spectrometer [Larmor frequencies 75.5 MHz (^{13}C), 59.6 MHz (^{29}Si) and 111.9 MHz (^{119}Sn)], using standard 7 and 4 mm CP MAS probes and a Bruker BVT-1000 temperature control unit. CP contact times of 0.5–1.5 (^{13}C), 5 (^{29}Si) and 1.0–1.5 ms (^{119}Sn), recycle delays of 7–20 s, and ^{1}H decoupling field strengths of 71 kHz were employed in standard CP MAS NMR experiments. The samples were contained in 7 or 4 mm o.d. (outside diameter) ZrO_2 rotors sealed with BN endcaps. MAS frequencies were generally in the range 3.0–4.0 kHz. The stability of the MAS frequencies was actively controlled to ± 2 Hz, using a home-built device. Several ^{13}C and ^{119}Sn MAS NMR exchange (EXSY) experiments CP–t_1–$\pi/2$–τ_{mix}–$\pi/2$–t_2 (Ernst *et al.*, 1987; Schmidt-Rohr & Spiess, 1994) with phase cycling according to the TPPI scheme (Marion & Wüthrich, 1983) were acquired for mixing times τ_{mix} ranging from 0.3 to 2 s; between 4 and 64 transients per t_1 increment had to be acquired for obtaining sufficiently good signal-to-noise ratio. No ^{1}H decoupling during τ_{mix} is employed in the standard version of the EXSY experiment. Isotropic chemical shifts are indicated relative to those of $SiMe_4$ (^{13}C, ^{29}Si) and $SnMe_4$ (^{119}Sn) according to the deshielding convention.

2.2. Experimental results

2.2.1. X-ray powder diffraction. Indexing with *ITO* (Visser, 1969) led to similar triclinic cells for (1) and (2), with the possible space groups $P1$ or $P\bar{1}$ and two molecules in the unit cells. The peak profiles and precise lattice parameters were determined by LeBail-type fits using the program *GSAS* (LeBail *et al.*, 1988; Larson & Von Dreele, 1994). The background was modeled manually using *GUFI* (Dinnebier & Finger, 1998). The peak profile was described by a pseudo-Voigt function, in combination with a special function that accounts for the asymmetry due to axial divergence (Thompson *et al.*, 1987; Finger *et al.*, 1994).

The crystal structure of (1) was solved using the DASH[1] structure solution package as follows: Data in the range $1 \leq 2\theta \leq 14.0°$ were subjected to a Pawley refinement (Pawley, 1981) in space group $P\bar{1}$ in order to extract 320 correlated integrated intensities from the pattern. A good fit to the data ($\chi^2 = 5.76$) was obtained. An internal coordinate description of the organic moiety in idealized T_d symmetry was constructed using standard bond lengths (Ge—Sn 2.7, Sn—C 2.15, C—H 0.95 Å) and four torsion angles for the trimethylstannyl groups (Fig. 1). These torsion angles could not be assigned precise values in advance and they were determined in the simulated annealing procedure. The position, orientation and conformation of the organometallic moiety in the refined unit cell were postulated and the level of agreement between the trial structure and the experimental diffraction data quantified by $\chi^2 = \sum_h \sum_k [(I_h - c|F_h|^2)(V^{-1})_{hk}(I_k - c|F_k|^2)]$, where I_h and I_k are Lorentz–polarization corrected, integrated intensities from the Pawley refinement of the diffraction data. V_{hk} is the covariance matrix from the Pawley refinement, c is a scale factor, and $|F_h|$ and $|F_k|$ are the structure factor magnitudes calculated from the trial structure. The trial structure was subjected to a global optimization (David *et al.*, 1998; Dinnebier, Wagner *et al.*, 2000), in which the four torsion angles were the only internal degrees of freedom and the external degrees of freedom consisted of three fractional coordinates describing the position of the molecule and four quaternions (Leach, 1996) describing its orientation. Examination of the structure giving the best fit to the data showed the molecules to form a distorted closed packing with the centers of mass being located very close to $\frac{3}{4}\ \frac{1}{4}\ \frac{1}{4}$ and $\frac{1}{4}\ \frac{3}{4}\ \frac{3}{4}$, respectively, in the triclinic unit cell. The structure giving the best fit to the data ($\chi^2 = 33.7$ at $T = 23.34$ K after 990 000 moves) was verified by Rietveld refinement of the fractional

[1] *DASH* is a product of the Cambridge Crystallographic Data Centre, 12 Union Road, Cambridge CB2 1EZ, England.

coordinates obtained at the end of the simulated annealing run.

Rietveld refinements for (1) and for the isostructural (2) were carried out in space groups $P\bar{1}$ and $P1$ using the *GSAS* program system (Rietveld, 1969; Larson & Von Dreele, 1994). Lowering the space group symmetry to $P1$ resulted in only minor improvements of the fit, establishing $P\bar{1}$ as the correct space group. To account for the scattering power of the H atoms of the methyl groups, the occupancy factor for the C atoms of the methyl groups was fixed to 1.5, as explained elsewhere (Dinnebier *et al.*, 1999). Rietveld refinements were first carried out using a rigid-body description for the molecular moiety of (1) (Dinnebier *et al.*, 1999; Dinnebier, 1999), allowing the refinement of the position and orientation of the molecule, the torsion angles of the trimethylstannyl groups and the overall Ge–Sn and Sn–C bond lengths, while keeping the tetrahedral symmetry of the molecule. Although the Rietveld refinement converged, differences between the observed and calculated profile indicated some distortions from the ideal molecular geometry. Since unconstrained refinement of molecular materials from powder diffraction data usually result in highly correlated parameters, 16 soft constraints for bond lengths and 30 soft constraints for bond angles were applied. The Rietveld refinement converged quickly to the R values given in Table 1. The positional parameters of the final Rietveld refinement and the isotropic temperature factors have been deposited.[2]

A first-order phase transition to a face-centered cubic (*f.c.c.*) phase occurred for (1) and (2) at 348 ± 5 K on heating and back to the triclinic phase at 350 ± 2 K upon cooling for (1) (Fig. 3). The phase transition is accompanied by a relative increase in volume of approximately 16% with respect to the volume of the low-temperature unit cell (Fig. 4). The thermal expansion of the triclinic low-temperature phase is very small, but increases considerably for the cubic high-temperature phase. It should be noted that owing to the different experimental setup for the high-temperature experiment, the uncertainty in determining the unit-cell parameters is much higher than for the high-resolution experiment at low temperature. Owing to the high rotational disorder of the molecules of (1) and (2) in their high-temperature phases, the molecules appear to be almost perfect spheres, which does not allow the determination of individual atomic positions. Rather than individual atomic scattering factors, spherical shell form factors modelled by symmetry-adapted Bessel functions can be used as in the case of C_{60} (*e.g.* Margadonna *et al.*, 1999). For the description of a perfect sphere, spherical harmonics of first order are sufficient: $F_{hkl} = \sum_{i=1}^{n}[f_i(\sin Qr_i/Qr_i)]$, which is the sum over all n atoms belonging to the molecule, with the structure factor F of the reflection hkl, the amount of the reciprocal vector Q and the distance r_i of the ith atom to the center of gravity of the molecule. A refinement using the program *FULLPROF* (Carvajal, 2001) shows a satisfactory fit (Fig. 5) and confirms the high degree of rotational disorder of (1) in the high-temperature *f.c.c.* phase. A more detailed description of the non-uniform distribution of electron density requires higher-order spherical harmonics, which will be the subject of another paper.

2.2.2. NMR. ^{119}Sn and ^{13}C MAS NMR spectra of $Ge(SnMe_3)_4$ (1) are shown in Fig. 6. Since ^{119}Sn MAS NMR alone cannot distinguish between intra- and intermolecular inequivalent tin sites, we cannot immediately assign the four ^{119}Sn resonances observed at $T = 190$ K as originating from four inequivalent $SnMe_3$ groups per $Ge(SnMe_3)_4$ molecule. However, additional inspection of the ^{13}C MAS NMR spectra

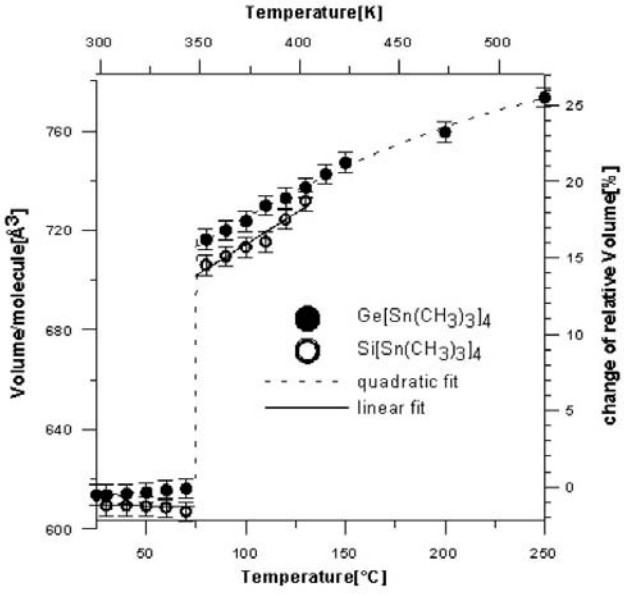

Figure 4
Volume per molecule in dependence of the temperature for (2) (open circles) and (1) (closed circles). The first-order phase transition around 348 K is clearly visible. As a guide to the eye, the data of (1) were fitted by a straight line (solid line), whereas the data of (2) were fitted by a quadratric function (dashed line). The slightly negative slope for the low-temperature phase of (1) can be attributed to experimental uncertainties.

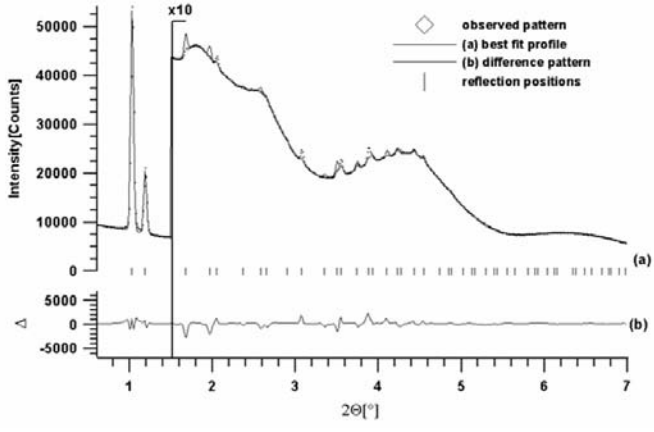

Figure 5
Rietveld refinement of the high-temperature phase of (1) at 353 K using spherical harmonics of first order. The highly structured background is caused by rotational disorder.

[2] Supplementary data for this paper are available from the IUCr electronic archives (Reference: OS0078). Services for accessing these data are described at the back of the journal.

of (1) at $T \simeq 150$ K to $T \simeq 220$ K does immediately rule out molecular T_d symmetry. If there were four independent molecules per asymmetric unit and if each molecule would have T_d symmetry, the number of ^{13}C resonances could never exceed the number of ^{119}Sn resonances and there would have to be one ^{119}Sn and one ^{13}C resonance per molecule. Even if the ^{13}C MAS NMR spectra of (1) (Fig. 6) are only poorly resolved, it is still obvious that these ^{13}C NMR spectra must represent more than four different, though incompletely resolved, ^{13}C resonances. By returning to the multiplicities and relative intensities of the resonances in the ^{119}Sn MAS NMR spectra of (1) at different temperatures, we can further narrow down the possible molecular symmetries. For example, the approximately equal intensities of the four ^{119}Sn resonances at $T \simeq 190$ K would not be consistent with two independent molecules, each with C_3 molecular symmetry, in the asymmetric unit. The most likely explanation is that there is one $Ge(SnMe_3)_4$ molecule in the asymmetric unit and that it lacks all symmetry, *i.e.* belongs to point group C_1.

Further independent (NMR) proof of the presence of at least two independent $SnMe_3$ groups per $Ge(SnMe_3)_4$ molecule is presented in Fig. 7, where the contour plot of a two-dimensional ^{119}Sn MAS EXSY experiment on (1) is shown, obtained at $T = 298$ K with a mixing time $\tau_{mix} = 300$ ms. This contour plot clearly displays exchange between the two spectrally resolved regions in the room-temperature ^{119}Sn MAS NMR spectrum of (1) (*cf.* second trace from top in Fig. 6). A two-dimensional ^{119}Sn MAS EXSY control experiment with ^{1}H decoupling applied during τ_{mix} showed identical off-diagonal peaks and thus excludes proton-driven ^{119}Sn spin diffusion (Ernst *et al.*, 1987; Schmidt-Rohr & Spiess, 1994) as the origin of the observed off-diagonal peaks in the spectrum depicted in Fig. 7. Since no indication of molecular orientational disorder exists from X-ray diffraction, only (slow) chemical exchange between inequivalent $SnMe_3$ groups within a $Ge(SnMe_3)_4$ molecule can cause this exchange pattern. This chemical exchange requires whole-molecule rotational jumps of the $Ge(SnMe_3)_4$ molecules in the crystal structure. Before discussing further the molecular dynamic properties of (1), we note that a two-dimensional ^{119}Sn MAS EXSY experiment at $T = 190$ K (where four ^{119}Sn resonances are resolved) would, in principle, be able to distinguish between a single, completely asymmetric molecule in the asymmetric unit and the presence of two independent molecules with some symmetry each. Unfortunately, in practice, the molecular dynamics of (1) at $T = 190$ K are so slow that in a two-dimensional ^{119}Sn MAS EXSY experiment at this temperature no significant intensity of ^{119}Sn exchange peaks is observed, not even with a mixing time as long as $\tau_{mix} = 2$ s. Qualitatively speaking, reorientational jumps of the $Ge(SnMe_3)_4$ molecules around their main molecular Ge–Sn axes do occur in the crystal structure, but these reorientational jumps are infrequent events in the low-temperature phase of (1).

We still need to explain the 'evolution' of the one-dimensional ^{119}Sn and ^{13}C MAS NMR spectra of (1) as a function of temperature (see Fig. 6) and need to consider the absence or presence of molecular dynamic processes, such as whole-molecule jumps or internal $2\pi/3$ reorientation of individual $SnMe_3$ groups in more detail. Since there is no indication of any orientational molecular disorder in the low-temperature phase of (1) from the X-ray diffraction results, two-dimensional ^{119}Sn MAS EXSY experiments on (1) at $T = 298$ K must probe the *intramolecular* exchange between inequivalent $SnMe_3$ sites. Consideration of the integrated relative off-diagonal intensities observed when using different mixing times τ_{mix} in two-dimensional ^{119}Sn MAS EXSY experiments (spectra not shown) permitted us to *estimate* an upper limit for the exchange rate constant(s) $\kappa_{ij} \leq 2$ s^{-1} at $T = 298$ K. In other words: whole-molecule reorientational jumps *are* rare events in the low-temperature phase of (1), and they are also rare on the corresponding one-dimensional ^{119}Sn NMR time scale and thus cannot be responsible for the temperature dependence of the isotropic ^{119}Sn chemical shifts observed in the temperature range T = 150–300 K. Instead, these small temperature-

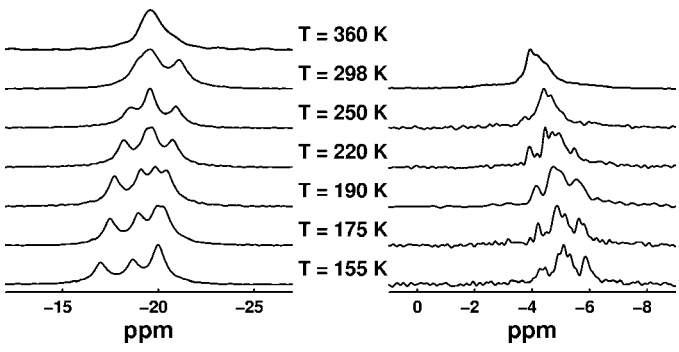

Figure 6
^{119}Sn (left) and ^{13}C (right) MAS NMR spectra of $Ge(SnMe_3)_4$ (1) at different temperatures, as indicated.

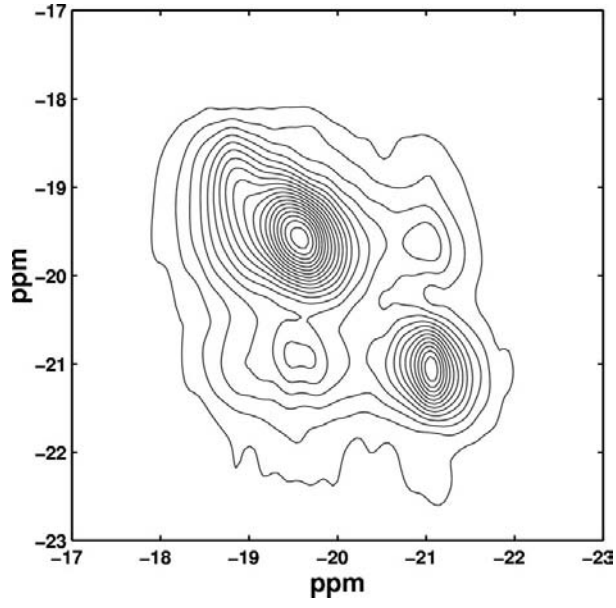

Figure 7
Contour plot of a two-dimensional ^{119}Sn MAS NMR EXSY experiment on $Ge(SnMe_3)_4$ (1), obtained at $T = 298$ K and with a mixing time $\tau_{mix} = 300$ ms.

Table 2
Selected intra- and intermolecular distances and angles of the ordered low-temperature structures of (1) and (2) at 295 K.

Realistic standard deviations are of the order 0.1° for the angles and 0.04 (Å) for the bond lengths according to Hill & Cranswick (1994); Rietveld statistical estimates are multiplied by a factor of six.

	$Ge(SnMe_3)_4$ (1)	$Si(SnMe_3)_4$ (2)
Distances (Å)		
$E-E_{min}$ intermolecular	8.91	9.02
Close-packed layer distance	7.26	7.26
$E-Sn$	2.58–2.62	2.53–2.58
$Sn-C$	2.16–2.18	2.11–2.24
$C-C_{min}$ intramolecular	3.53	3.43
$C-C$ intermolecular	3.81	3.98
Angles (°)		
Sn,Si/Ge,Sn	108.3–110.4	107.7–111.3
Trimethylstannyl Sn	109.0–109.7	108.9–112.0
Sn,Si/Ge,Sn,C (average)	58.6–61.7	56.9–61.6

dependent shifts (of the order between 0.08 and 0.02 p.p.m. K^{-1}) reflect the minor intrinsic dependence of chemical shielding on temperature and may slightly shift individual resonances to either higher or lower shielding values as a function of temperature. Similar temperature dependencies of isotropic ^{119}Sn chemical shifts are, for instance, observed for solid $C(SnMe_3)_4$ (Bernatowicz *et al.*, 1999). The one- and two-dimensional ^{119}Sn MAS NMR spectra of (1) do not provide any information regarding the absence or presence of internal $2\pi/3$ reorientation of the individual $SnMe_3$ groups. These dynamic processes, if present, are reflected in the temperature dependence of the ^{13}C methyl resonances (in addition to the effects of whole-molecule reorientational jumps). Given that $2\pi/3$ reorientation of individual $SnMe_3$ groups could be faster or slower than whole-molecule jumps at a given temperature, and that the activation energy of this process could be higher or lower than the activation energy for whole-molecule jumps in the crystal structure, it is quite impossible to make any reasonable semi-quantitative conjectures about the $2\pi/3$ reorientation of individual $SnMe_3$ groups from inspection of the variable-temperature ^{13}C MAS NMR spectra of (1) (see Fig. 6). In particular, the necessarily large number of incompletely resolved ^{13}C resonances [12 resonances for a $Ge(SnMe_3)_4$ molecule with C_1 symmetry] renders quantification impossible in this case. However, we can state with certainty the following. The two-dimensional ^{119}Sn MAS EXSY experiment at T = 190 K (mixing time τ_{mix} = 2 s) shows no significant exchange between tin sites. Similarly, a two-dimensional ^{13}C MAS EXSY experiment at T = 190 K (mixing time τ_{mix} = 250 ms) showed no exchange between methyl sites. Accordingly, at T = 190 K both whole-molecule and internal $2\pi/3$ reorientational jumps of individual $SnMe_3$ groups in (1) are absent on these rather long time scales. We cannot exclude the possibility that at temperatures T > 190 K eventually the internal reorientation of the various $SnMe_3$ groups in (1) may become thermally activated and we know that at T = 298 K whole-molecule reorientational jumps of (1) occur with exchange rate constant(s) $\kappa_{ij} \leq 2\ s^{-1}$.

A fairly similar overall picture to what we find for (1) is obtained from variable-temperature ^{29}Si, ^{119}Sn and ^{13}C MAS NMR spectra of (2). Over the temperature range T = 170–290 K, ^{29}Si MAS NMR spectra of (2) display a single, sharp ^{29}Si resonance which gradually shifts from $\delta_{iso}(^{29}Si)$ = −179.0 p.p.m. at T = 170 K to $\delta_{iso}(^{29}Si)$ = −175.7 p.p.m. at T = 290 K, and which is flanked by (unresolved) satellites due to J coupling, $^1J_{iso}(^{29}Si, ^{117/119}Sn) \simeq 214$ Hz. Over this temperature range, also for (2) there are always more than one, although poorly resolved ^{119}Sn resonances, and a number of nearly unresolved ^{13}C resonances (Fig. 8). Similar to the findings for (1), two-dimensional ^{119}Sn MAS EXSY experiments on (2) at T = 200 K and T = 250 K (τ_{mix} = 500 ms) showed the absence of chemical exchange between tin sites brought about by whole-molecule jumps of $Si(SnMe_3)_4$ molecules at these temperatures. Also similar to the findings for (1), the relative

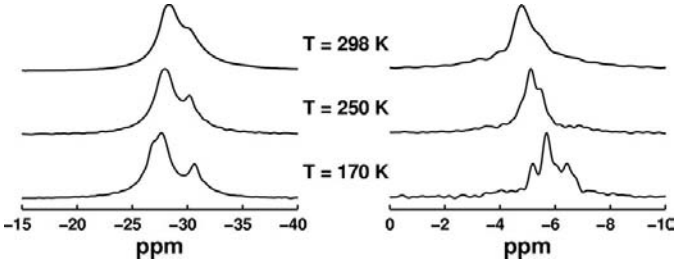

Figure 8
^{119}Sn (left) and ^{13}C (right) MAS NMR spectra of $Si(SnMe_3)_4$ (2) at different temperatures as indicated.

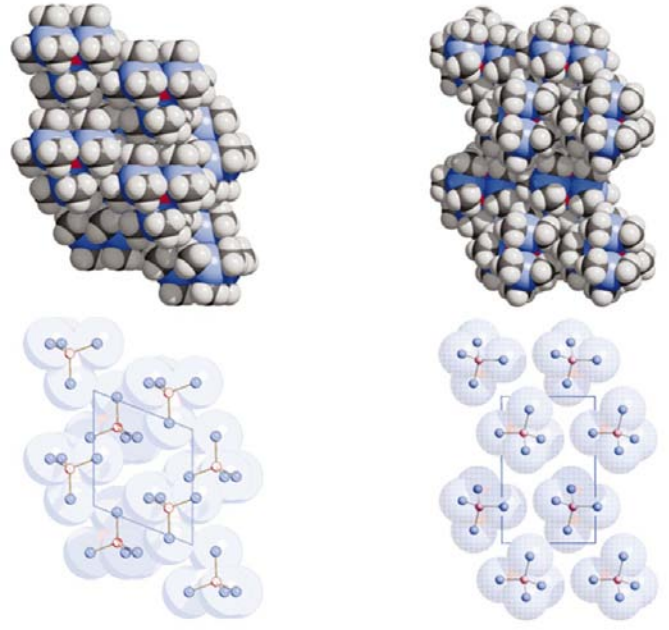

Figure 9
Cup models (with ball-and-stick representation inside) of the $(Ge/Si)Sn_4$ tetrahedra of the low-temperature phase of (1) [or (2)] in [010] (left) and [001] (right) directions, visualizing the pseudo-hexagonal close packing in this direction. On the bottom, the methyl groups were omitted for clarity. The *ABAB* stacking with the inverted tetrahedra in alternate layers are clearly visible.

intensities and number of (nearly unresolved) ^{13}C resonances at low temperatures exceed the number of ^{119}Sn resonances, so that also for (2) molecular T_d symmetry can be ruled out. Beyond this statement, it is impossible to define more accurately the (lack of) molecular symmetry of (2), owing to the rather limited spectral resolution in both the ^{13}C and ^{119}Sn MAS NMR spectra. If we take the observation of a single sharp ^{29}Si MAS NMR resonance for (2) as a reliable indication for the presence of only one silicon site in the asymmetric crystallographic unit, then the simultaneous observation of several ^{13}C and ^{119}Sn MAS NMR resonances is positive proof that the molecular symmetry of (2) in its low-temperature phase must be lower than T_d. Even if MAS NMR spectra generally are very sensitive to changes in short-range geometry, the rather small overall chemical shift range of the isotope ^{29}Si downscales this statement somewhat, as very minor differences in geometry at the silicon sites may not necessarily be translated into spectrally resolved isotropic ^{29}Si chemical shifts.

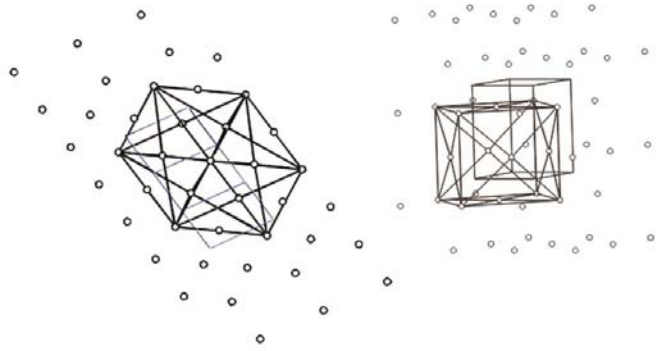

Figure 10
Center of gravity representation of the low-temperature phases of (1) and (2), showing only the central Ge (Si) atoms in [210] (left) and [10,1,15] (right) view direction. The triclinic unit cell (thin lines) as well as the corresponding F-centered *pseudo*-orthorhombic unit cells are shown, the latter indicating the mechanism of the triclinic to *f.c.c.* phase transformation. The (210) plane of the low-temperature phase corresponds to the close-packed (111) planes in the *f.c.c.* lattice of the high-temperature phase.

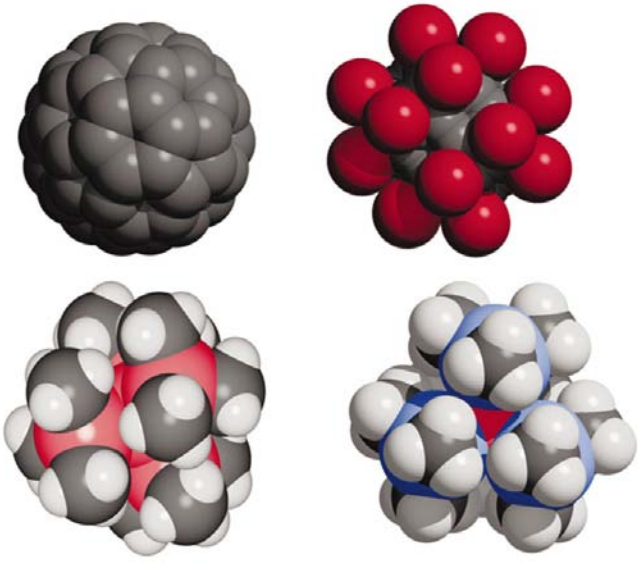

Figure 11
Comparison of the shape of four quasispherical molecules C_{60} (top, left), $C_{60}Br_{24}$ (top, right), $C(SiMe_3)_4$ (bottom, left) and $Ge(SnMe_3)_4$ (bottom, right).

3. Discussion

The X-ray diffraction experiments (see Figs. 2, 3 and 5) clearly confirm a low crystallographic symmetry and low molecular symmetry for the isotypic low-temperature phases of (1) and (2) (Table 2). In neither of the two triclinic space groups $P1$ or $P\bar{1}$ are there any symmetry restrictions on the individual molecules, allowing the four $SnMe_3$ groups of one molecule to orient independently from each other. Although the deviations from molecular T_d symmetry are relatively small (Table 2), they are considered to be significant, because the Rietveld refinements using the perfect T_d or T symmetry led to considerably higher R values than refinements where no *a priori* symmetry restrictions were applied. From this finding, it may be concluded that the molecular symmetry of (1) and (2) in their low-temperature phases is C_1. This differs from the findings for the ordered low-temperature phases of $C(SiMe_3)_4$ and $Si(SiMe_3)_4$, where the molecular symmetry is C_3 (Dinnebier *et al.*, 1999).

For both compounds (1) and (2), the positions of the molecules are close to $\pm(\frac{1}{4}\ \frac{1}{4}\ \frac{3}{4})$. The crystal structures of the low-temperature phases can be described as a stacking of distorted closed-packed layers (angle of 112° rather than 120°) along the crystallographic b axis (Fig. 9). The molecules within the layers have their trimethylstannyl groups nested. Consecutive layers are shifted by $\frac{1}{2}\ \frac{1}{2}$ forming a *b.c.c.*-like (body-centered cubic) *ABAB* type of packing (Fig. 9). The 'thickness' of the layers is given by half the length of the b axis (Table 2). This finding suggests that a possible high-temperature phase may adopt either a *h.c.p.* (hexagonal closed packing) or a *c.c.p* (cubic closed packing) structure by shifting consecutive layers along $(\mathbf{a} + \mathbf{b})$ about $(1/6)|\mathbf{a} + \mathbf{b}|$. Indeed, a first-order phase transition towards a *f.c.c.* phase was observed for both (1) and (2) at 348 ± 5 K. This phase transition is accompanied by a relative increase in unit-cell volume of approximately 16% with respect to the volume of the low-temperature unit cell.

Interestingly, the mechanism of the observed phase transition is not as expected. This can be seen by comparing the *F*-centered cubic unit cell of the high-temperature phase to the *F*-centered *pseudo*-orthorhombic unit cell which can be derived directly from the triclinic low-temperature unit cell. The conversion matrix from triclinic to *pseudo*-orthorhombic is given by

$$\begin{pmatrix} 1 & -1 & 0 \\ 1 & 1 & 0 \\ 0 & 0 & 1 \end{pmatrix},$$

accompanied by a shift of origin of

$$\begin{pmatrix} \frac{1}{4}(\mathbf{x}-\mathbf{y}) \\ 0 \\ \frac{1}{4}\mathbf{z} \end{pmatrix}$$

(Fig. 10). For (1) this leads to lattice parameters of the pseudo-orthorhombic unit cell at room temperature of $a' = 15.82$, $b' = 10.74$, $c' = 14.53$ Å, $\alpha' = 89.6$, $\beta' = 90.3$, $\gamma' = 84.9^\circ$. From Fig. 10 it is evident that the close-packed layers, which are aligned perpendicular to [111] in the *f.c.c.* lattice, are aligned perpendicular to the [210] rather than perpendicular to the [010] direction in the triclinic unit cell. During the phase transition the crystallographic symmetry of the individual molecules increases considerably, which must be explained by a high degree of disorder. The major change in the *pseudo*-orthorhombic lattice during the phase transition to a *f.c.c.* lattice occurs in the *b* direction, which increases by ∼4 Å, whereas the *a* axis shrinks by ∼1.3 Å and the *c* axis remains about the same.

For both compounds (1) and (2) the shortest distance between the centers of gravity of the molecules increases from ∼9.0 Å in the low-temperature phases at 298 K to ∼10.0 Å in the high-temperature phases at 353 K. Accordingly, the distance of the close-packed layers increases from $b/2 \simeq 7.3$ Å in the low-temperature phases at 298 K to $(3^{1/2}/3)a \simeq 8.2$ Å in the high-temperature phases at 353 K. Although the crystallinity decreases rapidly with increasing temperature, even at 523 K the basic features of an *f.c.c.* lattice are visible in the X-ray powder diffraction pattern.

With the number of isotropic ^{119}Sn and ^{13}C resonances in MAS NMR spectra directly reflecting the number of crystallographically independent tin and carbon sites in the asymmetric unit and in the absence of orientational disorder, NMR also arrives at the conclusion that the molecular point-group symmetry C_1 is by far the most likely explanation for the $Ge(SnMe_3)_4$ molecules in the low-temperature phase of (1). The results of solid-state NMR and X-ray diffraction experiments not only agree with regard to the presence of low molecular symmetry in (1); both methods further independently arrive at the conclusion that the degree of distortion from an ideal tetrahedral molecular geometry in (1) must be very small (see Table 2). From the viewpoint of NMR, this conclusion rests on the general NMR properties of heavy spin-1/2 isotopes. Heavy NMR-active isotopes such as ^{119}Sn usually cover chemical shift ranges of several thousand p.p.m. in a range of chemical environments and hence are particularly sensitive probes for detecting small changes in local geometry by changes in the chemical shifts (Sebald, 1994). Only a very small geometric distortion of the $Ge(SnMe_3)_4$ molecules from tetrahedral is consistent with the very small differences in ^{119}Sn chemical shifts found for the low-temperature phase of (1). Note that our combined solid-state NMR and X-ray diffraction results are at variance with the interpretation of the vibrational spectra of the low-temperature phase of (1) as being indicative of molecular T_d symmetry by Leites *et al.* (1999).

A difference in perception between NMR and X-ray diffraction regards the transition to the high-temperature phase of (1). The ^{119}Sn CP MAS NMR spectrum of (1) taken at $T = 360$ K and thus well above the transition temperature of (1) to its high-temperature phase indicates a gradual merging of the ^{119}Sn resonances into one, still broadened resonance (Fig. 6). In contrast, this phase transition reveals itself as a fairly spectacular sudden increase in the unit-cell dimensions when observed by powder X-ray diffraction, as illustrated in Figs. 3 and 4. Both findings taken together indicate that at this phase transition the crystal packing of the molecules is profoundly changed, whereas the molecular geometry of (1) is affected only to a minor extent. The transition does not seem to be related with a change of the dynamical behavior of the molecules.

The low-temperature phases of (1) and (2) further expand the wide range of structural and dynamic solid-state properties of compounds $E(XMe_3)_4$ towards the low-symmetry and little-motion end of the scale in this class of chemicals. It can be concluded that the degree of 'sphericalness' of these non-polar molecules is not only responsible for the packing of these molecules in crystals, but also for the type of phase transitions occurring. For the almost perfectly spherical molecules C_{60} (Chow *et al.*, 1992) and $C(SiMe_3)_4$ (Dinnebier *et al.*, 1999; Fig. 11) the transition from the rotationally disordered high-temperature phases to the 'neighbouring' low-temperature phase proceeds from $Fm\bar{3}m$ to $Pa\bar{3}$. The high molecular rigidity and the molecular inversion symmetry of C_{60} does not necessitate further reduction of space-group symmetry in order to arrive at a fully ordered structure. In contrast, at even lower temperatures $C(SiMe_3)_4$ and $Si(SiMe_3)_4$, with less rigid and symmetric molecular moieties, proceed to the space group $P2_13$ in which a fully ordered low-temperature phase structure is finally possible. The less spherically shaped molecules $Ge(SnMe_3)_4$ (1) and $Si(SnMe_3)_4$ (2) might be compared with compounds such as $C_{60}Br_{24}$ molecules in the fully bromine-saturated C_{60} derivative (Dinnebier *et al.*, 1995; Fig. 11). All three show high symmetry in their high-temperature phases. Whereas the title compounds (1) and (2) possess a perfect *f.c.c.* lattice, $C_{60}Br_{24}$ exhibits a rhombohedral crystal structure which is only slightly distorted from *f.c.c.* due to some interstitial bromine molecules. All three compounds undergo phase transitions to triclinic structures which can be viewed as more or less distorted *f.c.c.* lattices.

4. Conclusions

Using high-resolution X-ray powder diffraction and MAS NMR, it was possible to fully characterize the molecular and crystal structures of the low- and high-temperature phases of $Ge(SnMe_3)_4$ and $Si(SnMe_3)_4$. In particular, the simulated annealing technique for the determination of molecular crystal structures from powder diffraction proved to be a powerful tool which will soon become routine.

It can be concluded that the balance between intra- and intermolecular optimization of the molecular conformation in the solid state is the main reason for the different behavior of $Si(SiMe_3)_4$ (Dinnebier *et al.*, 1999) and $Si(SnMe_3)_4$ with

respect to their dynamic properties, phase transitions and molecular symmetry in the ordered low-temperature phases.

In a more general context, vibrational spectroscopy seems to bear the danger of overestimating the molecular symmetry of solid phases $E(X\mathrm{Me}_3)_4$ (Leites *et al.*, 1999). Instead, the combined experimental evidence from high-resolution powder X-ray diffraction and MAS NMR rules out molecular point-group symmetry T_d for the low-temperature phases of (1) and (2): both techniques indicate a complete lack of molecular symmetry for (1) and (2), with a small but significant amount of distortion from regular tetrahedral molecular geometry. The complementary character of high-resolution X-ray diffraction and NMR techniques applied to polycrystalline powder samples provides powerful combined constraints for the interpretation of experimental results. While X-ray diffraction indicates a fully ordered crystal structure at room temperature and disorder in the high-temperature phase, NMR shows that reorientational jumps of the molecules persist well into the low-temperature phase and that they gradually become less frequent on decreasing temperature.

We thank L. A. Leites and V. Ya. Lee, Moscow, for the donation of our sample of $\mathrm{Si(SnMe_3)_4}$ (2). Special thanks are due to José Merino (ID15B) for his assistance during the measurements. Diffraction measurements at ESRF were carried out under the general user proposals CH-846 and HS1295. Financial support by the Deutsche Forschungsgemeinschaft (DFG), the Fonds der chemischen Industrie (FCI) and the guest program of Bayerisches Geoinstitut (BGI) is gratefully acknowledged. XH and AS thank Aventis Pharma, Paris, for financial support.

References

Beagley, B., Pritchard, R. G. & Titiloye, J. O. (1988). *J. Mol. Struct.* **176**, 81–87.

Beagley, B., Pritchard, R. G. & Titiloye, J. O. (1989). *J. Mol. Struct.* **212**, 323–324.

Bernatowicz, P., Dinnebier, R. E., Helluy, X., Kümmerlen, J. & Sebald, A. (1999). *Appl. Magn. Reson.* **17**, 385–398.

Carvajal, J. R. (2001). *FullProf*2k, Version 1.9c, LLB JRC; available at ftp://charybde.saclay.cea.Fr/pub/divers/fullprof.2k/.

Chow, P. C., Jiang, X., Reiter, G., Wochner, P., Moss, S. C., Axe, J. D., Hanson, J. C., McMullan, R. K., Meng, R. L. & Chu, C. W. (1992). *Phys. Rev. Lett.* **69**, 2943–2946.

Cox, D. E (1991). *Handbook of Synchrotron Radiation*, edited by G. Brown & D. E. Moncton, Vol. 3, ch. 5. Amsterdam: Elsevier.

David, W. I. F., Shankland, K. & Shankland, N. (1998). *Chem. Commun.* pp. 931–932.

Dinnebier, R. E. (1999). *Powder Diffr. J.* **14**, 84–92.

Dinnebier, R. E., Carlson, S. & van Smaalen S. (2000). *Acta Cryst.* B**56**, 310–316.

Dinnebier, R. E., Dollase, W. A., Helluy, X., Kümmerlen, J., Sebald, A., Pagola, S., Stephens, P. W. & van Smaalen, S. (1999). *Acta Cryst.* B**55**, 1014–1029.

Dinnebier, R. E. & Finger, L. (1998). *Z. Kristogr.* Suppl. 15, 148; available at http://www.pulverdiffraktometrie.de.

Dinnebier, R. E., Stephens, P. W., Carter, J. K., Lommen, A. N., Heiney, P. A., McGhie, A. R., Brard, L. & Smith III, A. B. (1995). *J. Appl. Cryst.* **28**, 327–334.

Dinnebier, R. E., Wagner, M., Peters, F., Shankland, K. & David, W. I. F. (2000). *Z. Anorg. Allg. Chem.* **626**, 1400–1405.

Ernst, R. R., Bodenhausen, G. & Wokaun, A. (1987). *Principles of Nuclear Magnetic Resonance in One and Two Dimensions.* Oxford: Clarendon Press.

Finger, L. W., Cox, D. E. & Jephcoat, A. P. (1994). *J. Appl. Cryst.* **27**, 892–900.

Hammersley, A. P. (1997). ESRF97HA02T, FIT2D: *An Introduction and Overview.* ESRF Internal Report.

Hammersley, A P. (1998). ESRF98HA01T, FIT2D V9.129 *Reference Manual*, V3.1. ESRF Internal Report.

Helluy, X., Kümmerlen, J. & Sebald, A. (1998). *Organometallics*, **17**, 5003–5008.

Hill, R. J. & Cranswick, L. M. D. (1994). *J. Appl. Cryst.* **27**, 802–844.

Klinkhammer, K. W., Kühner, S., Regelmann, B. & Weidlein, J. (1995). *J. Organomet. Chem.* **496**, 241–243.

Langford, J. I. & Louër, D. (1996). *Rep. Prog. Phys.* **59**, 131–234.

Larson, A. C. & Von Dreele, R. B. (1994). *GSAS*. Los Alamos National Laboratory Report LAUR 86–748; available by anonymous FTP from mist.lansce.lanl.gov.

Leach, A. R. (1996). *Molecular Modelling Principles and Applications*, p. 384. New York: Addison Wesley Longman Ltd.

LeBail, A., Duroy, H. & Fourquet, J. L. (1988). *Mater. Res. Bull.* **23**, 447–452.

Leites, L. A., Bukalov, S. S., Garbuzova, I. A., Lee, V. Ya., Baskir, E. G., Egorov, M. P. & Nefedov, O. M. (1999). *J. Organomet. Chem.* **588**, 60–68.

Margadonna, S., Brown, C. M., Prassides, K., Fitch, A. N., Knudsen, K. D., Le Bihan, L., Mézouar, M., Hirosawa, I. & Tanigaki, K. (1999). *Int. J. Inorg. Mater.* **1**, 157–163.

Marion, D. & Wüthrich, K. (1983). *Biochem. Biophys. Res. Commun.* **113**, 967–974.

Parsonage, N. G. & Staveley, L. A. K. (1978). *Disorder in Crystals.* Oxford: Clarendon Press.

Pawley, G. S. (1981). *J. Appl. Cryst.* **14**, 357–361.

Rietveld, H. M. (1969). *J. Appl. Cryst.* **2**, 65–71.

Schmidt-Rohr, K. & Spiess, H. W. (1994). *Multidimensional Solid-State NMR and Polymers.* London: Academic Press.

Sebald, A. (1994). *NMR Basic Principles and Progress*, edited by B. Blümich, Vol. 31, pp. 91–131. Berlin: Springer-Verlag.

Suortti, P., Buslaps, T., Honkimäki, V., Shukla, A. & Kretzschmer, M. (2001). To be published.

Thompson, P., Cox, D. E. & Hastings, J. B. (1987). *J. Appl. Cryst.* **20**, 79–83.

Visser, J. W. (1969). *J. Appl. Cryst.* **2**, 89–95.